

Biodegradable LC Oligomers with Cranked Branching Points Form Highly Oriented Fibrous Scaffold for Cytoskeletal Orientation

Tatsuo Kaneko, Hang Thi Tran, Michiya Matsusaki, and Mitsuru Akashi*

Department of Applied Chemistry, Graduate School of Engineering, Osaka University, 2-1 Yamadaoka, Suita, 565-0871 Japan

Received July 10, 2006. Revised Manuscript Received October 26, 2006

Thermotropic liquid crystalline (LC) hyperbranch oligoesters (molecular weight of ca. 8 kDa) composed of rigid biodegradable segments, oligo{4-hydroxycinnamic acid (4HCA)}, plus a multifunctional biomolecule, cholic acid (CA), were prepared. Semiempirical calculations for the most stable conformation of the model compound CA derivatives with four arms of 4HCA tetramer showed that every arm can adopt an almost parallel orientation and that the CA unit can form a crankshaft architecture and function as a four-way junction of a branch point. Oligo(4HCA-co-CA)s successfully form molecularly oriented fibers with a high orientation degree by spinning viscous LC melts. Scanning electron microscopy demonstrated that mouse fibroblasts oriented uniaxially along the fiber longitudinal axis. Moreover, confocal fluorescence scanning microscopy showed that the RFP-stained cytoskeleton of these fibroblasts oriented highly.

Introduction

Living tissues have an innate structure with an orientation order, under which biological functions are facilitated in the living body.¹ Orientation control in tissues cultivated in vitro is indispensable for tissue revival engineering. However, the control of cell orientation is so difficult that only uniaxial orientations have been possible using structural adjustments of the cell-culture substrate.^{2–4} On the other hand, one of the most effective methods for controlling the substrate orientation on the molecular level is to use thermotropic liquid crystalline (LC) polymers.⁵ However, conventional LC polymers are composed of toxic components⁶ and therefore unsuitable for use as substrata for cell cultivation. We then synthesized linear LC polyesters from bioderived monomers such as 4-coumaric acid (4HCA)⁸ and lithocholic acid (LCA),⁹ but the molecular weights of the LC polyesters were

less than 8000 Da. The linear polymers composed of 4HCA and other bioderived comonomers showed a good cell compatibility and degradability because of the low molecular weight.^{9,10} The copolymers with the low molecular weight, i.e., oligoester, had difficulty creating the oriented material because there was no special interchain interaction such as physical interaction and/or entanglement. The chain entanglement can be enhanced by the hyper-branching architecture.¹¹ Here, we select a multifunctional bioderived comonomer, cholic acid (CA), and show the preparation of nontoxic LC oligoesters with hydrolytic short segments from multifunctional metabolite molecules under the concept of “cranked branching” formation; the oligoesters are then used to form molecularly oriented biofibers. Moreover, cells cultivated on these biofibers showed cell and cytoskeleton orientations along the biofiber axis, confirmed by scanning electron microscopy and confocal scanning microscopic observation of the stained cytoskeleton. The use of molecularly oriented biofibers for tissue construction can lead to the formation of oriented cell tubes such as vessels and nerves following the LC fiber biodegradation.

Experimental Section

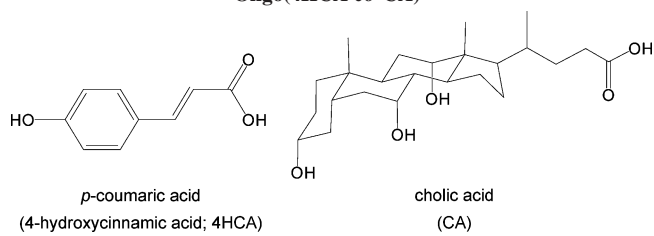
Materials. 4-Coumaric acid {4HCA; Tokyo chemical industry (TCI)} and cholic acid (CA; Wako Pure Chemical Industries, Ltd.) monomers were used as received. Acetic anhydride (Wako Pure Chemical Industries, Ltd.) and sodium acetate (Wako Pure Chemical Industries, Ltd.) used for the oligomerization were used as received. Acetone (Wako Pure Chemical Industries, Ltd.) used as a washing solvent was also used as received. Trifluoroacetic acid-d (TFA-d; TCI) and dichloromethane (DCM-d2) were obtained from Wako Pure Chemical Industries, Ltd.

* To whom correspondence should be addressed. Fax: 81-6-6879-7359. Tel: 81-6-6879-7356. E-mail: akashi@chem.eng.osaka-u.ac.jp.

† Current address: School of Materials Science, Japan Advanced Institute of Science and Technology, Asahidai, Nomi, 923-1292 Japan.

- (1) Porter, K. R.; Bonneville, M. A. *An Introduction to the Fine Structure of Cells and Tissues*, 2nd ed.; Lea & Febiger: Philadelphia, PA, 1964.
- (2) (a) Zhu, X.; Mills, K. L.; Peters, P. R.; Bahng, J. H.; Liu, E. H.; Shim, J.; Naruse, K.; Csete, M. E.; Thouless, M. D.; Takayama, S. *Nat. Mater.* **2005**, *4*, 403. (b) Balaban, N. Q.; Schwarz, U. S.; Riveline, D.; Goichberg, P.; Tzur, G.; Sabanay, I.; Mahalu, D.; Safran, D.; Bershadsky, A.; Addadi, L.; Geiger, B. *Nat. Cell. Biol.* **2001**, *3*, 466.
- (3) (a) Poole, K.; Khairy, K.; Friedrichs, J.; Franz, C.; Cisneros, D. A.; Howard, J.; Mueller, D. *J. Mol. Biol.* **2005**, *349*, 380. (b) Co, C. C.; Wang, Y. C.; Ho, C. C. *J. Am. Chem. Soc.* **2005**, *127*, 1598. (c) Clark, P.; Connolly, P.; Moores, G. R. *J. Cell. Sci.* **1992**, *103*, 287.
- (4) Kaneko, T.; Ogomi, D.; Mitsugi, R.; Serizawa, T.; Akashi, M. *Chem. Mater.* **2004**, *16*, 5596.
- (5) (a) Collings, P. J.; Hird, M. *Introduction to Liquid Crystals*; Taylor & Francis: London, 1997. (b) Chandrosskhar, S. *Liquid Crystals*, 2nd ed.; Cambridge University Press: Cambridge, U.K., 1992.
- (6) Somogyi, A.; Bojkova, N.; Padias, A. B.; Hall, H. K., Jr. *Macromolecules* **2005**, *38*, 4067.
- (7) Flory, P. J. *J. Am. Chem. Soc.* **1952**, *74*, 2718.
- (8) Kaneko, T.; Matsusaki, M.; Tran, H. T.; Akashi, M. *Macromol. Rapid Commun.* **2004**, *25*, 673.
- (9) Matsusaki, M.; Tran, H. T.; Kaneko, T.; Akashi, M. *Biomaterials* **2005**, *26*, 6263.

- (10) Matsusaki, M.; Kishida, A.; Stailon, N.; Christopher, W. G. A.; Akashi, M. *J. Appl. Polym. Sci.* **2001**, *82*, 2357.
- (11) Weng, W.; Markel, E. J.; Dekmezian, A. H. *Macromol. Rapid Commun.* **2001**, *22*, 1488.

Table 1. Synthetic Conditions and Properties of Oligo(4HCA-co-CA)^a


O=C(O)/C=C/c1ccc(O)cc1 CC(C)CC(O)CC(O)CC(O)C
p-coumaric acid cholic acid
 (4-hydroxycinnamic acid; 4HCA) (CA)

CB _{CAB} in feed ^b (mol %)	4HCA (mmol)	CA (mmol)	C _{CA} in co-oligomer ^b (mol %)	T _m ^c (°C)	T _i ^c (°C)	crystallization degree ^d (%)	yield ^e (wt %)
0	50	0	0	220	high	91	84
10	45	5	4	247	high	70	74
20	40	10	8	227	high	69	56
50	25	25	13	156	high	60	20
60	20	30	16	147	195	54	14
70	15	35	19	132	174	39	7
80	10	40	30	132	134		8
100	0	50	100				97

^a Oligomerization was carried out in the presence of acetic anhydride and sodium acetate with mechanical stirring for 6 h at 200 °C. 4HCA and CA refer to 4-coumaric acid and cholic acid, respectively. ^b C_{CA} refers to the molar composition of cholic acid to the total amount of monomers. ^c The melting temperature, T_m, and the isotropization temperature, T_i, were measured by crossed-polarizing microscopy equipped with a hot stage and differential scanning calorimetry. The word "high" represents T_i being too high to determine without thermal degradation. ^d The crystallization degree was measured from an X-ray diffraction diagram and a blank space represents data that could not be obtained because of small crystalline peaks. ^e The yield was measured after purification.

Syntheses. Oligo(4HCA-co-CA)s were synthesized by a two-step reaction in a one-pot synthesis by the following procedure. Monomers of 4HCA (8.0–0.0 g) and CA (0.0–20.4 g) were mixed and mechanically stirred at 150 °C in the presence of acetic anhydride (40 mL) as a condensation reagent, and trace amounts of sodium acetate as a transesterification catalyst were added until the solution became homogeneous (about an hour). The solution was further heated to 200 °C, and the oligomerization was carried out for another 6 h. The reaction solution increased its viscosity gradually and became light yellow. After the reaction was finished and cooled to room temperature, unreacted monomers were removed by washing with acetone, but the solution was not further purified. The results of synthesis and oligomer characterization are summarized in Table 1.

Molecular Weight Measurements. The molecular weight of the oligomers was determined by gel permeation chromatography (GPC; Shimadzu LC-6A system with a TSK-GEL Super H2000 column) that was calibrated with polystyrene standards (eluent: dimethylformamide).

Cell Adhesion. Oligo(4HCA-co-CA) disks were prepared in order to perform cell adhesion tests. A total of 40 mg of sample plus 10 μL of distilled water were added into a compressor holder and compressed under a vacuum at 300 kg/cm² for 5 min. After being molded, the disks (1 cm diameter and 0.4 mm height) were vacuum-dried for 24 h at room temperature. We then performed the L929 fibroblast cell adhesion test using these disks. Various disks were fixed onto 24-well multiplates by a stainless steel ring, and L929 cells were seeded onto the disks at 10 × 10⁴ cells/well. The cells were incubated for 24 h at 37 °C in Eagle's minimal essential medium (EMEM) containing 10% FCS and washed twice with phosphate buffered saline. The number of cells adhered onto the disks was counted with trypan blue staining on a hemocytometer.

Scanning Electron Microscopy. The morphology of the cells growing on the samples was studied by SEM as follows. Im-

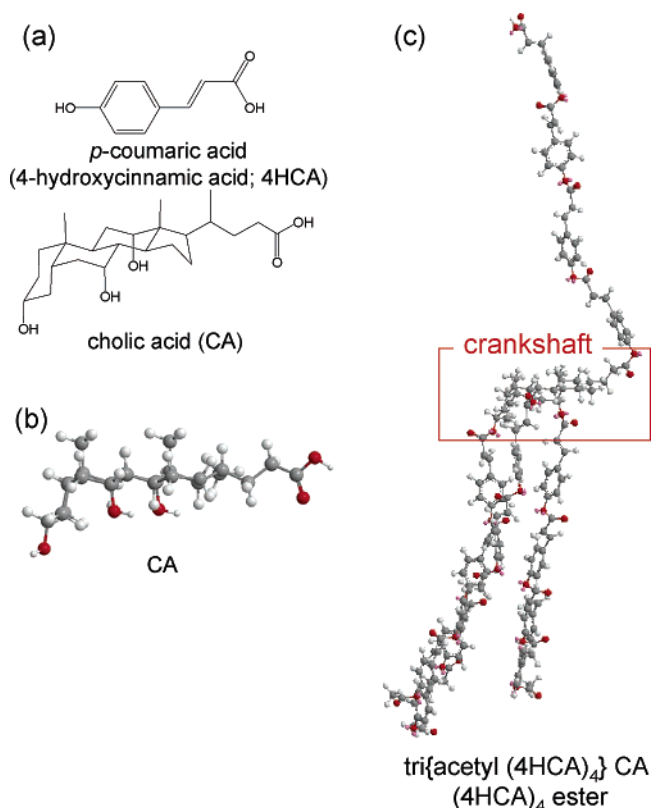


Figure 1. (a) Chemical structures of monomers. (b, c) Schematic ball-and-stick illustration for one of the most stable conformations of the poly-{*p*-coumaric acid (4HCA)-co-cholic acid (CA)} model compound calculated by MM2 and MOPAC. The white, gray, and red balls represent H, C, and O atoms, respectively. (b) CA; (c) tri{acetyl(4HCA tetramer)}CA (4HCA tetramer)ester; part c shows that the CA, marked by an open red quadrilateral, adopts the role of a branching point for four tetra-4HCA arms and forms a crankshaft structure.

mediately following the cell adhesion and proliferation tests, the samples were fixed with 3% GTA in PBS. After being washed in PBS, the fixed samples were dehydrated in ethanol (25, 50, 90, 95, 99.5%) and 2-methyl-2-propanol. The dehydrated samples were then freeze-dried and fixed onto a stage for SEM observation. Before the SEM observation was performed, osmium tetroxide was spattered onto the samples at a thickness of approximately 10 nm.

Confocal Fluorescence Scanning Microscopy Oligo(4HCA-co-CA) fibers were set onto a surface of TCPS, and L929 cells were seeded onto the fibers at 10 × 10⁴ cells/well. The cells were incubated for 7 days at 37 °C in EMEM containing 10% FCS and washed twice with phosphate buffered saline. The actin fibers of the adhering L929 cells were stained by phalloidin-tetramethylrhodamin B isothiocyanate (SIGMA), and the nuclei were stained by DAPI (Molecular Probes). The specimens were then observed by a slit disk scanning confocal microscope (Olympus).

Results and Discussion

CA has three hydroxyl groups on one side of the steroid area or the hydrophilic area, methyl groups on the hydrophobic reverse side area, and an aliphatic acidic group at the end, as shown in Figure 1a. This unique, multifunctional structure of CA can play a role in the branching point in the polymerized chains. Flory showed theoretically that the polymerization of AB_x type multifunctional monomers with one kind of functional group (A) and two or more (B) of another type created a hyperbranch architecture without

cross-linkage.⁷ CA is an AB₃ monomer, where A is carboxylic acid and B are the hydroxyls, and thus the co-oligomerization of CA with 4HCA cannot create a cross-linkage but rather a hyper-branching architecture. The synthesis of oligo(4HCA-co-CA) co-oligomers was performed in a manner similar to that for the 4HCA homooligomer⁸ and oligo(4HCA-co-LCA)s⁹ shown as follows. Monomers of 4HCA and CA were mixed and mechanically stirred at 150 °C in the presence of acetic anhydride as a condensation reagent and trace amounts of sodium acetate as a transesterification catalyst were added for about an hour. The solution was further heated to 200 °C, and the oligomerization was carried out for another 6 h. When the CA composition in the feed was increased, the yield of the co-oligomers decreased (see Table S1 in the Supporting Information). This may show a lower reactivity for CA than 4HCA. The increased solubility of the co-oligomers with an increased CA composition against the washing solvent of acetone could raise the amount of washed-out components from the products. The products were obtained as a yellowish powder. All the co-oligomers prepared here were dissolved in a mixed solvent of trifluoroacetic acid/dichloromethane (1/5 v/v), and the co-oligomers with a C_{CA} of 30 mol % and CA homooligomer were dissolved in acetone, acetonitrile, chloroform, dichloromethane, toluene, dimethylformamide (DMF), *N*-methylpyrrolidone, and tetrahydrofuran. The results of the solubility test demonstrated that the co-oligomer formed no cross-linkages, as expected. Co-oligomers showed a weight-average molecular weight (*M_w*) of 7000–8000 Da (polydispersity of ca. 1.4), which is sufficiently low to show the hydrolysis, as estimated by GPC measurements in DMF solution (polystyrene standard). The *M_w* was comparable to that of oligo4HCA (8000 Da from ¹H NMR) shown in a previous report.⁸

IR spectroscopy of oligo(4HCA-co-CA)s confirmed the presence of an acetyl ester group ($\nu_{\text{C=O}}$ 1762 cm⁻¹), coumaryloyl ester group ($\nu_{\text{C=O}}$ 1731 cm⁻¹), aromatic group ($\nu_{\text{p-}\phi}$ 1635 cm⁻¹), and alicyclic group ($\delta_{\text{C-H}}$ 1505 cm⁻¹), thus supporting an oligoester structure (see Figure S1a in the Supporting Information). The ¹N HMR spectra showed multiple peaks in the chemical shift range δ 6.65–8.09, assigned to phenylenevinylene protons, multiple peaks in the range δ 0.81–2.70, assigned to some steroidal aliphatic protons and acetate protons, and three peaks at δ 4.70, 5.05, and 5.30, assigned to the steroidal protons of C3, C7, and C12, respectively, which were attached at the O element (see Figure S1b in the Supporting Information). According to the literature,¹² the protons at C3, C7, and C12, with non-esterified hydroxyl groups, appeared in the chemical shift range of 3.5–4.0 ppm. On the other hand, the present ¹H NMR spectrum showed no peaks in this range, thus indicating that all of the hydroxyl groups were esterified. However, it was impossible to differentiate the signals due to the protons at these carbons from those due to coumaryloyl ester and acetyl ester. The literature has shown that the triacetylation of CA can be accomplished smoothly¹² but we were cautious because of the steric hindrance of the tricoumaryloyl esterification.

Next, we made a semiempirical calculation of the steric energy of the model compound, reflecting the branching point in the co-oligomers by a coupling method of MOPAC to MM2. Panels b and c of Figure 1 show a schematic ball-and-stick illustration (white ball, H; gray ball, C; red ball, O) for one of the most stable conformations of the model compounds. All of the calculated data are summarized in Table S1 of the Supporting Information. The most stable conformation of CA showed a planar steroid group in which all three hydroxyl groups project out almost perpendicularly and the carboxylic acid projects out almost in parallel to the steroid plane, as shown in Figure 1b (The heat of formation, $\Delta H = -298.3$ kcal mol⁻¹). First, we investigated the acetylation effects of CA on the ΔH value. If the hydroxyl group at the C3 carbon was acetylated to create O3-acetylcholic acid (mono-2), the ΔH value decreased slightly to -312.5 kcal mol⁻¹. On the other hand, acetylation of the hydroxyl group at C7 (mono-3) and C12 (mono-4) created less stable compounds ($\Delta\Delta H = 23.9$ and 25.9 kcal mol⁻¹, respectively). This result indicates the preference of C3 esterification, which is in good agreement with the experimental and theoretical results shown in the literature^{12,13} regarding CA esterification, thus supporting the present calculation method. The reason for this result is that only the hydroxyl group at the C3 position had an equatorial configuration of steroidal alicycles receiving less steric hindrance. Next, we found that the ΔH values for O3, O7, O12-triacetylcholic acid 4-coumaric acid ester were lower than that of O3, O7, O12-tri(4-acetoxy-cinnamoyl)cholic acid 4-coumaric acid ester (see Table S1 in the Supporting Information), indicating that the conversion from an acetyl into a *p*-coumaryloyl group was accomplished smoothly without any large steric hindrances. In the final calculation, the steric hindrance effects on the propagation of 4HCA branching were investigated. When the arms become CA tetra-substituted by the 4HCA tetramer (tetra-10), the ΔH value was very low (-33.7 kcal mol⁻¹), but higher than those of acetylated CAs (see Table S1 in the Supporting Information). These results indicate that the propagation can proceed smoothly. Figure 1c shows a ball-and-stick illustration of the most stable conformation for tetra-10. This illustration shows that the steroidal skeleton was not greatly deformed and that the three arms attached to the hydrophilic area projected out in a similar direction, with one arm attached at the carboxyl on the opposite side. All other model compounds having shorter arms than the tetra-10 showed a conformation similar to that of the tetra-10. The shape of the tetra-10 compound is like a triple crankshaft, and the CA is centered in a four-way junction of similarly directing arms. On the basis of the calculations of the model compounds, one can guess that the hyperbranch chains with a “cranked branch” architecture may be formed smoothly without any steric hindrance. The C_{CA} values of the model compounds used here were greater than 5.8%, and the structures around the branch points of the co-oligomers with C_{CA} values of 8, 13, 16, 18, and 30% may be similar to those of the model compounds. On the basis of the assumption of

(12) Baker, J. F.; Blickenstaff, R. T. *J. Org. Chem.* **1975**, *40*, 1579.

(13) Hu, X.; Zhang, Z.; Zhang, X.; Li, Z.; Zhu, X. X. *Steroids* **2005**, *70*, 531.

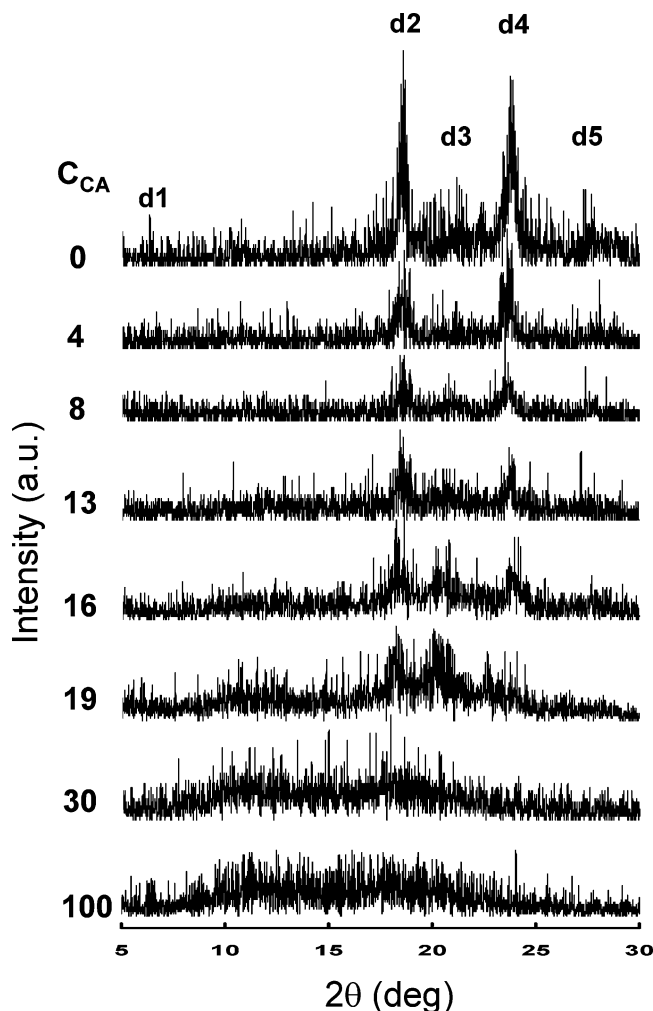


Figure 2. Wide-angle X-ray diffraction (WAXD) diagrams of the oligo(4HCA-co-CA)s. WAXD diagrams were recorded on an X-ray diffractometer (RINT UltraX18) equipped with a scintillation counter using Cu K α radiation (40 kV, 200 mA; wavelength = 1.5418 Å), which was monochromated by a parabolic multilayer mirror in transmission geometry.

homogeneous arm propagation, we can estimate the number of CA units (branch points) for LC oligomers with the molecular weight of 7000–8000 to be about 3 for 8%, 6–7 for 13%, 7–8 for 16%, 7–8 for 18%, and 9–11 for 30%.

To investigate the crystalline structure, we performed wide-angle X-ray diffraction (WAXD) studies of the co-oligomers (Figure 2). The 4HCA homooligomer showed four diffraction peaks at $2\theta = 10.8$ (d1), 17.0 (d2), 20.6 (d3), 23.0 (d4), and 28.8° (d5) (θ = diffraction angle), corresponding to spacings of 0.82, 0.49, 0.43, 0.38, and 0.31 nm, respectively. The WAXD pattern indicates that the 4HCA homooligomer is crystalline and aligned hexagonally with a distance of 0.98 nm, as described in a previous report.⁸ When the CA was co-oligomerized, the crystal diffraction peaks slightly shifted toward the smaller angle, became less intense, and were no longer detected in the co-oligomer with a CA composition of 30 mol % (only amorphous halo in $2\theta = 8$ –23°). The crystallization degree was 91% in the oligo4HCA, whereas those were at most 70% in the present co-oligomers, which decreased with an increase in the C_{CA} value (Table 1). CA incorporation into the 4HCA chains reduced both the crystallinity and the liquid crystallinity. Because the CA homooligomer is amorphous, the CA units

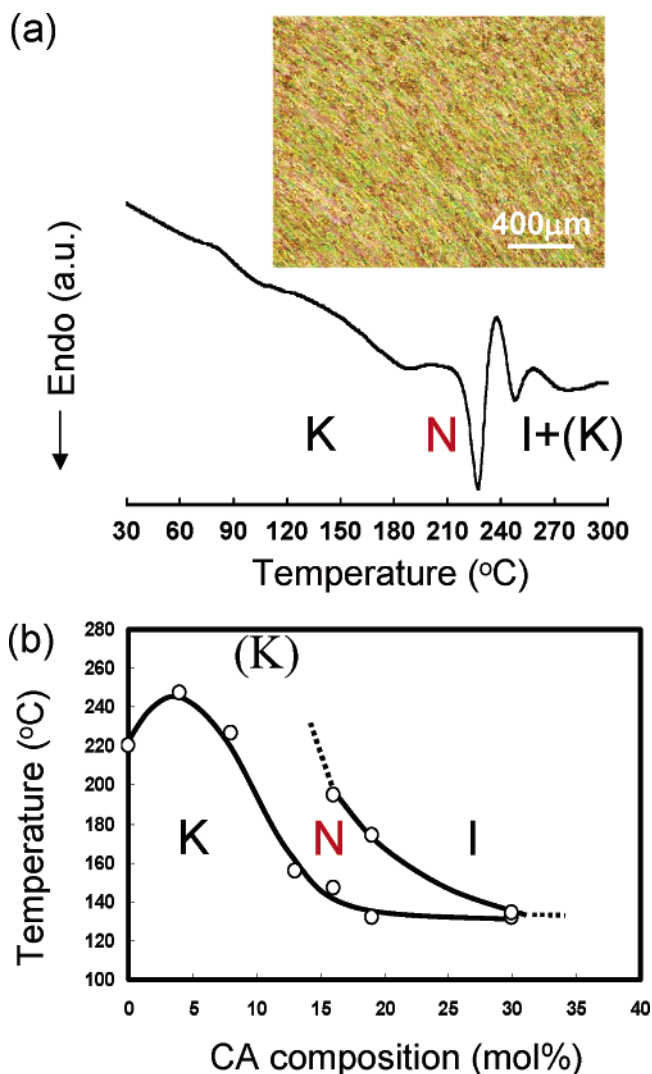


Figure 3. Thermotropic behavior of the oligo(4HCA-co-CA)s. (a) Representative differential scanning calorimetry (DSC; EXSTAR6100, Seiko Instruments Inc.) thermogram ($CB_{CAB} = 8\%$) upon heating. (b) Phase diagram was drawn on the basis of the results of DSC and crossed-polarizing microscope observation (Olympus BX51). The samples were sandwiched between two glass plates and heated at a rate of $10\text{ }^\circ\text{C min}^{-1}$ (resolution: $\pm 0.1\text{ }^\circ\text{C}$) by a METTLER TOLEDO FP82HT Hot Stage (Greifensee, Switzerland).

may disorganize the arrangement of the oligo4HCA rodlike arms. The cranked shape and branching structure both reduced the linearity of the oligomer chains, thus disturbing the regular arrangement.

To investigate the thermotropic properties of oligo(4HCA-co-CA)s, we performed crossed-polarizing microscopic observations coupled with DSC measurements. When the co-oligomer with a CA composition of 8% was heated at a rate of $10\text{ }^\circ\text{C min}^{-1}$ under microscopic observation, the sample was melted at $227\text{ }^\circ\text{C}$ to create a birefringent liquid that showed a banded texture (Figure 3a) typical of the nematic liquid crystalline state. This texture was repeatedly observed on successive thermal treatments. The isotropization temperature, T_i , appeared over a composition range of 16–30 mol %. As a consequence, the co-oligomer exhibited a nematic phase in which the oligomer chains were autonomously oriented but randomly located.⁵ On the basis of the results of the DSC and microscopic observations, we

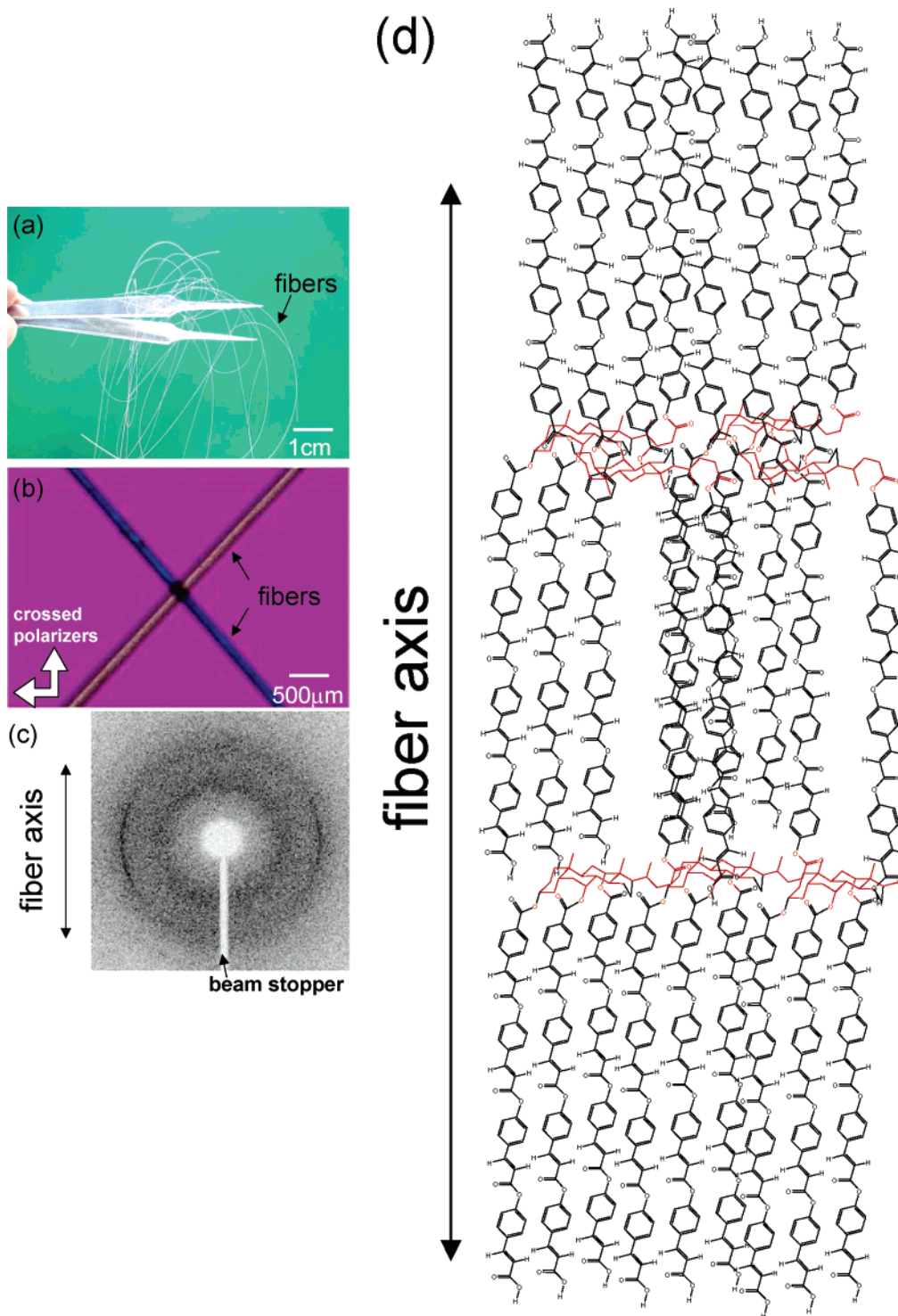


Figure 4. Structural analyses of the oligo(4HCA-co-CA) fiber spun from the nematic state. (a) Digital camera photograph of a representative fiber ($C_{CA} = 13\%$) supported by a pair of tweezers. (b) Crossed-polarizing microscopic (PLM) image of representative fibers ($C_{CA} = 13\%$) crossed at a 45° angle to both the polarizer and analyzer, taken in the presence of a sensitive color plate ($\lambda = 530$ nm). (c) Wide-angle X-ray diffraction (WAXD) image of the representative fiber ($C_{CA} = 13\%$). (d) Schematic illustration of the co-oligomer chain arrangement in the fiber generated from the results of PLM and WAXD. The CA units are colored red.

summarized the T_m and T_i values in Table 1 and show the phase diagram in Figure 3b.

The co-oligomers in the liquid crystalline state were more viscous than linear oligomers with a similar structure, such as the 4HCA homooligomer and oligo(4HCA-co-LCA)s. Next, we tried to spin the fibers in the liquid crystalline melt state; we picked up the surface of the co-oligomer melts in the liquid crystalline state with a pair of tweezers and pulled

them to yield fibers with a thickness of about $100\text{--}500$ μm . A picture of a representative fiber is shown in Figure 4a. Microscopic pictures of the fibers taken under a crossed-polarizer are shown in Figure 4b. The fibers were bright when they made a $\pm 45^\circ$ angle to both the polarizer and analyzer, and furthermore, the fibers clearly showed blue and orange colors in the presence of a sensitive color plate ($\lambda = 530$ nm) depending on the angle sign. This observation

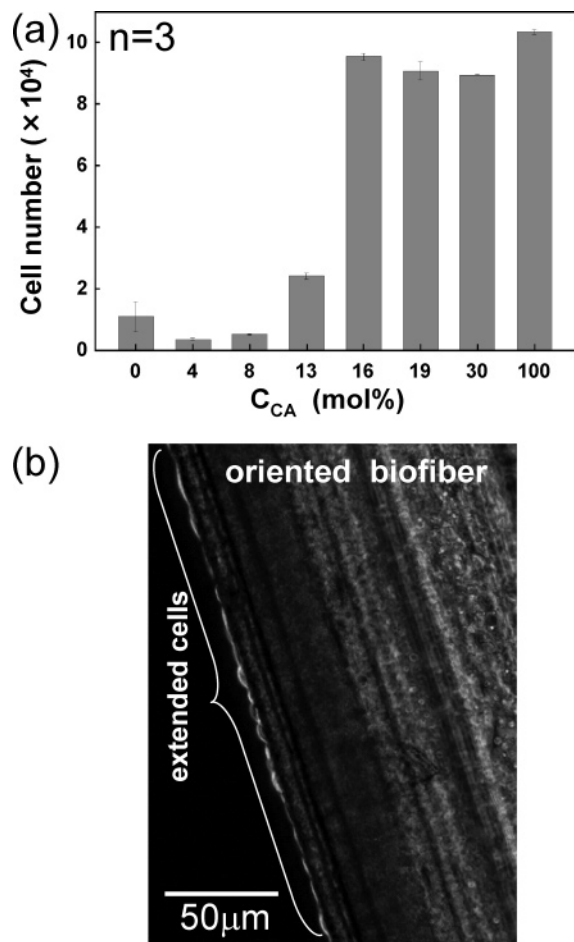


Figure 5. Mouse fibroblast (L929) adhesion behavior on a oligo(4HCA-co-CA) substrate. (a) CA composition dependence of the cell number adhering onto a co-oligomer pellet ($\phi = 10$ mm, thickness = 0.5 mm). (b) Differential interference microscopic (DIM) image of the cells adhering on oriented fibers of the co-oligomer with a C_{CA} of 19%. Only cells on the edge could be observed.

indicates that whole fibers were oriented homogeneously and that the birefringence value was negative, supporting the fact that the polymer chains were oriented along the fiber axis. Figure 4c shows representative XRD images of the fibers with a C_{CA} of 13 mol %, for which distinct diffraction arcs around $2\theta = 23^\circ$ on the equatorial line are apparent. This indicates that the present fibers were molecularly oriented. It was quite surprising that the fibers of molecularly oriented oligoester having no specific interchain interaction could be formed so easily, because the widely studied oriented polyester fiber was derived from the high-speed drawing of high-molecular-weight polymer melts. The cranked branching architecture can induce oligomer chain entanglement, which effectively increases the extensional viscosity.¹¹ The present orientation may be due to the specific structure of the four-way cranked branching point, as shown in Figure 4d, suggesting a hyperbranch architecture in which every arm orients along the fiber axis. These arms can behave as a rigid-rod bundle of polymeric chains, thus enabling their liquid crystalline properties to result in successful spinning of the fibers with a macroscopic molecule orientation.

We confirmed the good cell compatibility of the co-oligomers by a cell adhesion test. After L929 fibroblasts were incubated on poly4HCA and oligo(4HCA-co-CA) pellets, they extended as far as cells extended on tissue culture polystyrene (TCPS). Figure 5a shows that the number of extended cells increased dramatically when the C_{CA} value exceeded 13% and showed a nearly constant value above 18%. The cell number corresponded to the reciprocal of the melting point, indicating that the structural ordering was related to cell adhesion. On the fibers, cell extension was also observed by differential interference microscopy (DIM), although only those cells present on the fiber edge are shown

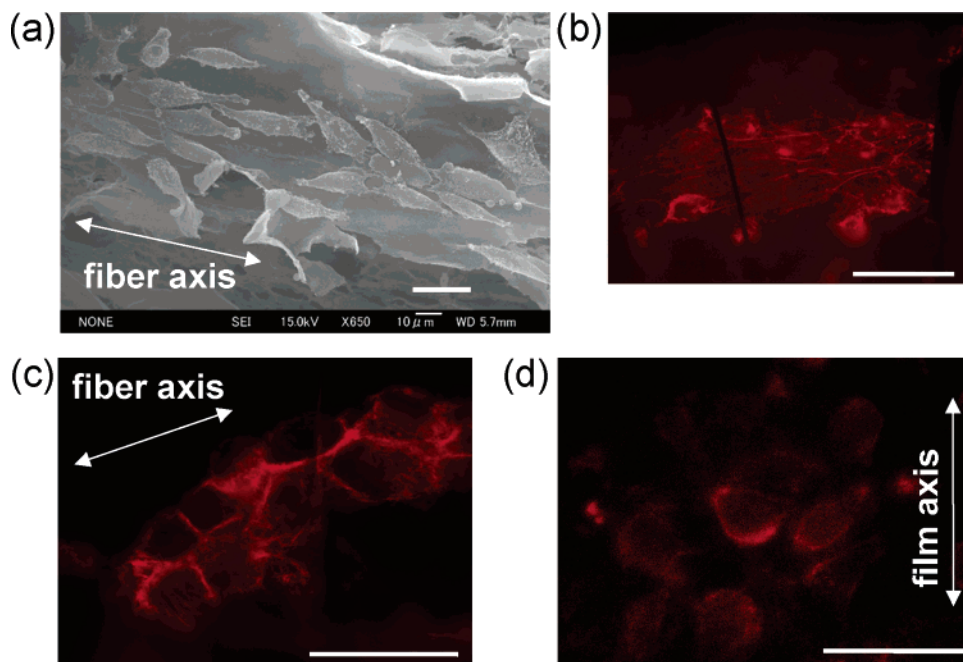


Figure 6. Microscopic images of mouse fibroblast (L929) adhering on various substrates. (a) Scanning electron microscopic (SEM) image on the oriented oligo(4HCA-co-CA) fiber with a C_{CA} of 19%. (b) Confocal fluorescence scanning microscopic (CFMSM) image on the oriented oligo(4HCA-co-CA) fiber with a C_{CA} of 19%. The cytoskeleton was stained by phalloidin-tetramethylrhodamin B isothiocyanate. (c) CFMSM image on the nonoriented biofiber of oligo(cholic acid) spun in the isotropic melt. (d) CFMSM image on an oriented film with a C_{CA} of 19% prepared using a pair of tweezers with the flat tips, in the nematic state. Scale bars = 20 μm .

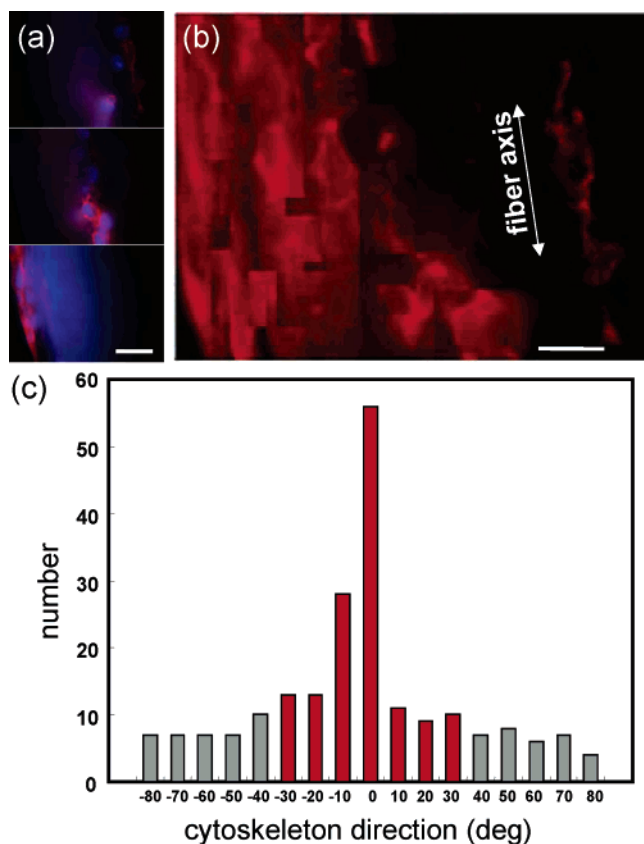


Figure 7. Cytoskeleton orientation analysis of mouse fibroblast (L929) adhered on the oriented fiber. (a) Representative CLSM video clips of the L929 fibroblasts adhered on oriented fibers of the oligo(4HCA-co-CA) with a C_{CA} of 19%. The video was taken while the Z-distance was continuously changed (see the Supporting Information, Video S1). (b) CLSM image of the L929 fibroblasts adhered on oriented fibers of the oligo(4HCA-co-CA) with a C_{CA} of 19%, which was created by a synthesis of the video clips mentioned in part a. The cell nuclei were removed for emphasis of the cytoskeletal structures. (c) The schematic illustration of the oriented cell adhered on the oriented fiber. (d) Frequency distribution of the cytoskeletal segment angles to the fiber axis. The cytoskeleton lines were divided into 220 segments at the folded points. The columns of the segments almost parallel to the fiber axis (within ± 30 degrees) were marked in red. Inset: schematic illustration of the cell morphology on the fiber. Scale bars = 20 μm .

in Figure 5b because of difficulty with focus adjustments for a round surface.

We then attempted to observe the cell morphology by scanning electron microscopy (SEM). One can observe that the extended cells were successfully oriented along the fiber axis (Figure 6a), although the substrate fiber was partly broken during the freeze-drying treatment. In order to observe the cell morphology without freeze-drying treatment, we observed the cytoskeletons stained by phalloidin-tetramethylrhodamin B isothiocyanate (RFP) using confocal fluorescence scanning microscopy (CFSM), and a representative CFSM image is shown in Figure 6b. The red lines of the cytoskeletons seemed to orient well along the fiber axis. On the other hand, no cytoskeleton orientation was observed in the cells extending onto the nonoriented fibers of oligoCA spun in the isotropic melt (Figure 6c) or onto the oriented films of the same polymer (Figure 6d). A comparison of

image b with images c and d of Figure 6 demonstrates that the cell extension orientation was not only derived from the molecular orientation but also from the cylindrical shape of the fibrous substrate. On the cylindrical substrate, the curved geometry may cause a negative effect on cell extension¹⁴ across the fiber axis, whereas no curvature appeared along the fiber axis.

Because all the cytoskeletons on the cylindrical substrate were not in focus by one shot, we recorded a movie of the cytoskeletons extending on the oriented fibers with gradual adjustment of the Z-distance (Video S1 in the Supporting Information). Figure 7a shows representative video clips of CFSM video (Video S1). One can clearly see that the RFP-stained cytoskeletons, seen as red lines, surround the DAPI-stained nuclei, seen as blue spheres. Figure 7b shows an image prepared by a synthesis of video clips, showing that the cytoskeletons were also well-oriented. From the microscopic image, the angle of the cytoskeletal lines to the fiber axis was analyzed, and about 220 data points were plotted in Figure 7d. Approximately 80% of the cytoskeleton is oriented almost parallel to the fiber axis (angle = $0 \pm 30^\circ$). To the best of our knowledge, many studies have previously reported a uniaxial orientation of the cells on a uniaxially pretreated substrate surface,^{2–4} with a two-dimensional geometry such as a sheet or plate. The microscopic pattern comprising cell-adhesive and cell-repulsive surfaces on the scaffold strongly affected the cell morphology.^{15–17} This patterning method is very effective on cell orientation but very complicated, whereas, in the process of LC spinning, a number of microscopic grooves may be formed on the surface of the oligo(4HCA-co-CA) fibers very easily (Figure 5b). The advantage of a one-dimensional fibrous substrate is the ease of orienting the cellular arrangement; for example, a cross arrangement of the biofibers causes the cells to grow in a cross-orientation. In addition, vascular endothelial cells oriented over the cylinder of the LC oligomer biofiber can generate an artificial capillary vessel following the fiber biodegradation.

Acknowledgment. This research was supported mainly by a Grant-in-Aid for NEDO (03A44014c) and Handai FRC and partly by Osaka University 21st Century COE Program “CENTER FOR INTEGRATED CELL AND TISSUE REGULATION”.

Supporting Information Available: Representative IR and ¹H NMR spectra of the oligo(4HCA-co-CA) and heat of formation of the model compounds obtained by MOPAC and MM2 calculations; representative video clips of CFSM. This material is available free of charge via the Internet at <http://pubs.acs.org>.

CM061573Z

- (14) Kaufmann, S.; Tanaka, M. *Chem. Phys. Chem.* **2003**, *4*, 699.
- (15) Mohammed, J. S.; DeCoster, M. A.; McShane, M. J. *Langmuir* **2006**, *22*, 2738.
- (16) Théry, M.; Pépin, A.; Dressaire, E.; Chen, Y.; Bornens, M. *Cell Motil. Cytoskeleton* **2006**, *63*, 341.
- (17) Raghavan, S.; Chen, C. S. *Adv. Mater.* **2004**, *16*, 1303.